Robust Backstepping Control of a Quadrotor UAV Under Pink Noise and Sinusoidal Disturbance

Mehmet KARAHAN*, Cosku KASNAKOGLU, Ahmet Nuri AKAY

TOBB University of Economics and Technology, 43 Sogutozu Street, Ankara, 06510, Turkey
m.karahan@etu.edu.tr (**Corresponding author*), kasnakoglu@etu.edu.tr, aakay@etu.edu.tr

Abstract: The new innovations in software and sensor technologies have facilitated the production of quadrotor unmanned aerial vehicles (UAVs) and expanded their area of use. Quadrotor UAVs are employed in a wide range of fields such as disaster relief, search and rescue, surveillance, mining, firefighting, crop dusting, product delivery, counterterrorism and photography. In order for the quadrotor to carry out these missions successfully, it must have a robust control structure. In this paper, a robust backstepping controller design that is resistant to pink noise and sinusoidal disturbance is proposed. Background noise in electronic devices is known as pink noise. The design of the background noise-tolerant controller is important as it improves the quadrotor's reference tracking performance. In the framework of this analysis, sinusoidal disturbance and pink noise were applied to the control structure of the selected quadrotor and its reference tracking performance was analysed. With the purpose of highlighting the superior features of the proposed backstepping control technique, the simulations that were carried out also involved the use of a PID controller and of a Lyapunov-based controller, and the results obtained for these controllers were compared with those obtained for the backstepping controller. As such, the time responses (rise time, settling time and overshoot) for the backstepping, PID and Lyapunov-based controllers were analysed. The obtained outcomes proved the superiority of the backstepping control design.

Keywords: Quadrotor, UAV, PID control, Lyapunov stability, Backstepping control, Sinusoidal disturbance, Pink noise, Robustness.

1. Introduction

Recent advances in sensor technologies, battery technologies, actuators and software technologies have facilitated the production of quadrotor unmanned aerial vehicles (UAVs) and led to their widespread use (Boukoberine et al., 2019; Aminifar & Rahmatian, 2020). Quadrotor UAVs' vertical takeoff and landing (VTOL) ability (Shraim et al., 2018), their low production cost (Xian et al., 2017), and their ability to perform harsh maneuvers (Al-Qrimli et al., 2021) make them more advantageous against winged UAVs. Quadrotor UAVs are used in many different fields for civil and military purposes today (Vanitha et al., 2020). Mapping, monitoring, border control, grain spraying, combating natural disasters, military use, intelligence and counterterrorism are among the important areas of use of quadrotors (Sabour et al., 2022; Yaacoub et al., 2020).

In the latest years, an increase has been observed in the number of studies on quadrotor unmanned aerial vehicles (Darvishpoor et al., 2020). In a number of recent studies, it can be seen that PID control design is widely preferred for altitude and attitude control of the quadrotor. The main reason for this situation is that the PID controller is widely used in this industry, its structure is simple, and the controller coefficients can be adjusted easily (Mahfouz et al., 2021). However, the PID controller does not fully meet robust control criteria. The robust controller is expected to be resistant to noise, parameter uncertainty and disturbances (Lucas et al., 2020). Many researchers focus on the design of a robust controller that is resistant to Gaussian noise and parameter uncertainty while designing controllers. However, the quadrotor may be exposed to different types of noise during operation. For example, colored noises, pink noise (background noise in electronic devices) are some of these noise types. In addition, the quadrotor may be subject to sinusoidal disturbance during operation. For this reason, there is a need for a controller design that is resistant not only to Gaussian noise and parameter uncertainty, but also to factors such as pink noise and sinusoidal disturbance.

Ma & Ji (2016) developed a fuzzy PID controller for the quadrotor space fixed-point position control and compared the results with those obtained by the traditional PID controller. Jiao et al. (2018) proposed a PID controller design for the attitude and position control of a quadrotor helicopter and tried to reduce the overshoot value by adjusting the control parameters. Li et al. (2021) used a PID control design and implemented a particle swarm optimization algorithm for controlling roll and yaw angles of the quadrotor. Noordin et al. (2020) developed a PID controller for a quadrotor and analysed its performance under Gaussian noise. Boudai et al. (2015) proposed an adaptive control technique for controlling altitude and position of

https://doi.org/10.24846/v32i2y202302

the quadrotor and made simulations under white Gaussian noise and parameter uncertainties. Tran et al. (2022) used a PID controller and observed the performance of the quadrotor under sensor noise and wind gust. They considered sensor noise as high sampling rates of white Gaussian noise and considered wind gust as low sampling rates of this noise. Antonelli et al. (2018) proposed an adaptive control and focused on the quadrotor trajectory tracking issue of the quadrotor under parameter uncertainties. Guardeño et al. (2019) used a PID control design for the altitude and position control of the quadrotor and added parametric uncertainty to the system inertia. Li et al. (2020) designed a robust controller for the tracking problem of the quadrotor under uncertain inertia and aerodynamic damping parameters.

In this study, a nonlinear model of a quadcopter was designed using the MATLAB software. After the model was created, the controller design part was followed. First of all, the PID and Lyapunov-based controller designs are explained. Then, the proposed backstepping control design was implemented for controlling the height, roll, pitch and yaw of the quadcopter. The backstepping controller is based on a recursive version of Lyapunov stability theorem. For this reason, it is expected to show a more robust performance than the Lyapunov-based controller and the classical PID controller. The proposed backstepping controller was tested under pink noise and sinusoidal disturbance, and the results were compared with those obtained for the Lyapunov-based controller and PID controller. Time response data for these three controllers with pink noise and sinusoidal disturbance were obtained and a comparative robustness analysis was performed. As a result of this analysis, it has been numerically proven that the backstepping controller is more robust than Lyapunov-based and PID controllers.

The remainder of this work is organized as follows. Section 2 describes the nonlinear quadrotor model. In Section 3, the design of the classical PID controller, Lyapunov-based controller and the proposed backstepping controller are discussed. In Section 4, simulations under pink noise and sinusoidal distortion are presented. Thanks to the numerical data obtained, the robustness of the employed controllers was compared and analyzed. Section 5 sets forth the conclusion of this paper.

2. The Quadrotor Model

The employed quadrotor is a four-propeller, VTOL UAV. It has two configurations, plus configuration and cross configuration. In this study, the cross configuration was used. In this configuration, the rotors (1,3) and (2,4) rotate oppositely. Increasing or reducing speed of all rotors simultaneously causes vertical directional motion. Changing speed of the 1st and 3rd rotors conversely results a roll movement. Changing speed of the 2nd and 4th rotor oppositely causes a pitch movement. Rotating the (1,3) and (2,4) pairs of rotors oppositely creates the yaw movement (Karahan & Kasnakoglu, 2021). The schematic representation of the quadrotor is given in Figure 1. In Figure 1, rotors rotating in the same direction are illustrated in the same color.

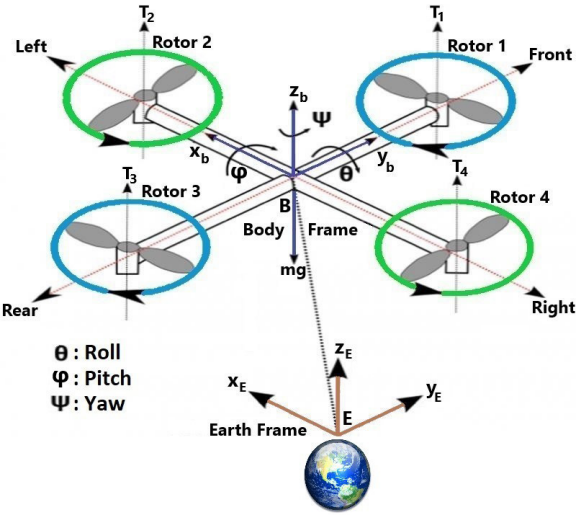

Figure 1. Representation of the employed quadrotor (Karahan & Kasnakoglu, 2021)

The rotation matrix is used to transform the Earth-centered frame into a body-centered frame. Equations (1) to (4) are used in this conversion. c symbolizes cosine and s symbolizes sine in equations.

$$R(\varphi)=\begin{bmatrix}1 & 0 & 0\\ 0 & c(\varphi) & s(\varphi)\\ 0 & -s(\varphi) & c(\varphi)\end{bmatrix} \quad (1)$$

$$R(\theta)=\begin{bmatrix}c(\theta) & 0 & -s(\theta)\\ 0 & 1 & 0\\ s(\theta) & 0 & c(\theta)\end{bmatrix} \quad (2)$$

$$R(\psi)=\begin{bmatrix}c(\psi) & s(\psi) & 0\\ -s(\psi) & c(\psi) & 0\\ 0 & 0 & 1\end{bmatrix} \quad (3)$$

$$R(\varphi,\theta,\psi)=R(\varphi)R(\theta)R(\psi) \quad (4)$$

Equation (5) gives the orthogonal rotation matrix R, which transforms the body-centered axis into an Earth-centered axis.

$$R=\begin{bmatrix} c\psi c\theta & s\psi c\theta & -s\theta \\ c\psi s\theta s\varphi - s\psi c\varphi & s\psi s\theta s\varphi + c\psi c\varphi & c\theta s\varphi \\ c\psi s\theta c\varphi + s\psi s\varphi & s\psi s\theta c\varphi - c\psi s\varphi & c\theta c\varphi \end{bmatrix} \quad (5)$$

Equations (6) and (7) show the transformation from body to Earth angular rates. p, q and r represent angular velocity components in body coordinates. $\dot{\varphi}$, $\dot{\theta}$ and $\dot{\psi}$ are Earth angular rates. tan represents tangent, sec represents secant in equations (6) and (7) below.

$$T=\begin{bmatrix} 1 & \tan(\theta)s(\varphi) & \tan(\theta)c(\varphi) \\ 0 & c(\varphi) & -s(\varphi) \\ 0 & \sec(\theta)s(\varphi) & \sec(\theta)c(\varphi) \end{bmatrix} \quad (6)$$

$$\begin{bmatrix} \dot{\varphi} \\ \dot{\theta} \\ \dot{\psi} \end{bmatrix} = T \begin{bmatrix} p \\ q \\ r \end{bmatrix} \quad (7)$$

Equation (7) for the derivatives requires that $\theta \neq \frac{\pi}{2}$. While φ and θ are close to 0, which means that UAV is hovering, T is nearly a unit matrix. In such a situation, the relation between angles and angular velocity components could be calculated as linear as in equation (8):

$$\begin{bmatrix} \dot{\varphi} \\ \dot{\theta} \\ \dot{\psi} \end{bmatrix} \approx \begin{bmatrix} p \\ q \\ r \end{bmatrix} \quad (8)$$

Force and torque formulas are given in equations (9) and (10), respectively. The i in the equations represents the rotor number from 1 to 4. w represents the angular velocity, b is thrust constant and d gives drag constant. Equation (11) represents the relative speed of rotor.

$$F_i = bw_i^2 \quad (9)$$

$$T_i = dw_i^2 \quad (10)$$

$$w_r = -w_1 + w_2 - w_3 + w_4 \quad (11)$$

Equation (12) gives the transition from controller inputs to angular velocities. U_1, U_2, U_3 and U_4 are control inputs, l is arm length of the quadrotor UAV. U_1 gives lift force and U_2, U_3, U_4 symbolize relevant torques.

$$u=\begin{bmatrix} U_1 \\ U_2 \\ U_3 \\ U_4 \end{bmatrix} = \begin{bmatrix} F \\ T_\varphi \\ T_\theta \\ T_\psi \end{bmatrix} = \begin{bmatrix} b & b & b & b \\ 0 & -lb & 0 & lb \\ lb & 0 & -lb & 0 \\ -d & d & -d & d \end{bmatrix} \begin{bmatrix} w_1^2 \\ w_2^2 \\ w_3^2 \\ w_4^2 \end{bmatrix} \quad (12)$$

Equation (13) describes the transition from angular velocities to controller inputs.

$$\begin{bmatrix} w_1^2 \\ w_2^2 \\ w_3^2 \\ w_4^2 \end{bmatrix} = \begin{bmatrix} 1/4b & 0 & 1/2bl & -1/4d \\ 1/4b & -1/2bl & 0 & 1/4d \\ 1/4b & 0 & -1/2bl & -1/4d \\ 1/4b & 1/2bl & 0 & 1/4d \end{bmatrix} \begin{bmatrix} U_1 \\ U_2 \\ U_3 \\ U_4 \end{bmatrix} \quad (13)$$

The moments of inertia of the quadrotor UAV are given in equations (14)-(16). M_{sphere} represents the mass of the spherical dense center, r symbolizes the radius, M_{rotor} is the mass of the rotor and l gives arm length of the quadrotor (Zabidin et al., 2020).

$$I_x = \frac{2}{5}M_{sphere}r^2 + 2l^2M_{rotor} \quad (14)$$

$$I_y = \frac{2}{5}M_{sphere}r^2 + 2l^2M_{rotor} \quad (15)$$

$$I_z = \frac{2}{5}M_{sphere}r^2 + 4l^2M_{rotor} \quad (16)$$

Figure 2 illustrates the masses of the quadrotor.

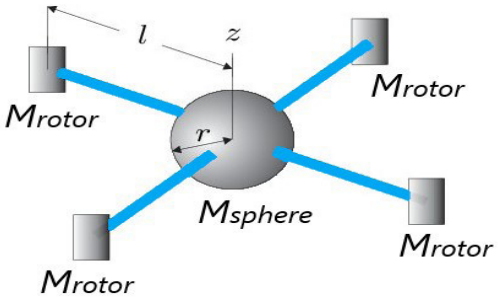

Figure 2. Illustration of the masses of the quadrotor

Nonlinear equations of motion of quadrotor at 6 degrees of freedom are given below.

$$\ddot{X} = \frac{U_1}{m}[c(\varphi)s(\theta)c(\psi) + s(\varphi)s(\psi)] \quad (17)$$

$$\ddot{Y} = \frac{U_1}{m}[s(\theta)s(\psi)c(\varphi) - s(\varphi)c(\psi)] \quad (18)$$

$$\ddot{Z} = -g + \frac{U_1}{m}[c(\varphi)c(\theta)] \quad (19)$$

$$\ddot{\varphi} = \frac{1}{I_x}U_2 + (\frac{I_y - I_z}{I_x})\dot{\psi}\dot{\theta} + w_r\frac{J_R}{I_x}\dot{\theta} \quad (20)$$

$$\ddot{\theta} = \frac{1}{I_y}U_3 + (\frac{I_z - I_x}{I_y})\dot{\theta}\dot{\psi} + w_r\frac{J_R}{I_y}\dot{\varphi} \quad (21)$$

$$\ddot{\psi} = \frac{1}{I_z}U_4 + (\frac{I_x - I_y}{I_z})\dot{\theta}\dot{\varphi} \quad (22)$$

Properties of OS4 quadcopter which is used in this paper are presented in Table 1.

Table 1. Quadrotor Properties

Property	Value
Overall mass (m)	0.65 kg
Gravity constant (g)	9.81 m/s^2
Arm length of quadrotor (l)	0.23 m
Max. rotor velocity (w_{max})	1000 rad/sec
Maximum torque (t_{max})	0.15 Nm
Thrust constant (b)	3.13x10^{-5} Ns^2
Drag constant (d)	7.5x10^{-7} Ns^2
Inertia moment on x axis (I_x)	7.5x10^{-3} kg.m^2
Inertia moment on y axis (I_y)	7.5x10^{-3} kg.m^2
Inertia moment on z axis (I_z)	1.3x10^{-2} kg.m^2
Rotor inertia (J_R)	6.5x10^{-5} kg.m^2

3. Controller Designs

In this section, the PID controller, Lyapunov-based controller and backstepping controller designs are explained.

3.1 PID Controller Design

In this part, the classical PID control is presented. PID controller has proportional (K_p), integral (K_i) and derivative (K_d) terms. PID controller tries to minimize error e(t) by using a control signal u(t). A general control equation could be written as in equation (23).

$$u(t) = K_p e(t) + K_i \int_0^t e(\tau) d\tau + K_d \frac{de(t)}{dt} \tag{23}$$

The controller input U_1 that controls the altitude is expressed in equation (24).

$$U_1 = \frac{m(g + e_z K_p + K_i \int e_z dt + K_d \frac{de_z}{dt})}{\cos\varphi \cos\theta} \tag{24}$$

In the above equation, θ angle corresponds to rotation around y axis and φ angle is rotation around x axis. Since the quadrotor UAV does not rotate in the x-axis and y-axis during vertical flight, the denominator of the U_1 control input will never be 0.

The U_2 control input controls the roll angle, the U_3 control input controls the pitch angle, and the U_4 control input controls the yaw angle. Equations (25) to (27) express these control inputs.

$$U_2 = e_\varphi K_p + K_i \int e_\varphi dt + K_d \frac{de_\varphi}{dt} \tag{25}$$

$$U_3 = e_\theta K_p + K_i \int e_\theta dt + K_d \frac{de_\theta}{dt} \tag{26}$$

$$U_4 = e_\psi K_p + K_i \int e_\psi dt + K_d \frac{de_\psi}{dt} \tag{27}$$

Table 2 presents PID controller's coefficients.

Table 2. PID controller coefficients

Coefficient	Roll	Pitch	Yaw	Altitude
K_p	0.12	0.14	0.13	0.82
K_i	0.05	0.07	0.05	0.1
K_d	0.06	0.08	0.1	1.65

3.2 Lyapunov-Based Controller Design

Lyapunov-based control is a nonlinear control approach based on Lyapunov stability theory (Babaie et al., 2022). In this subsection, the design of the Lyapunov-based controller is explained step by step. Lyapunov-based controller aims directly at controlling the position of UAV. In Lyapunov control method, x = 0 is the determined point of equilibrium. D is defined as a compact space of f(0) in R^n. The continuous Lyapunov equation V: D → R+ that satisfies requirements in equations (28) and (29) is defined.

$$V(0) = 0,\ V(x) > 0 \quad in\ \ D,\quad x \neq 0 \tag{28}$$

$$\dot{V}(x) \leq 0 \ \ in\ \ D \tag{29}$$

Point of equilibrium is asymptotically stable in D domain under $\dot{V}(x) \leq 0 \ \ in \quad , x \neq 0$ conditions. Next, a part, that contains stabilization angles and their derivates, is defined as desired attitude at point of equilibrium for the purpose of attitude control. In this case, $x = (\varphi_d, 0, \theta_d, 0, \psi_d, 0)$ where φ_d, θ_d and ψ_d, are defined as the desired roll, pitch and yaw. Due to the fact that angular velocity components will be 0 at the point of stabilization, their derivatives will be 0. Positively defined Lyapunov equation at desired position is given in equation (30):

$$V(x) = \frac{1}{2}[\dot{\varphi}^2 + (\varphi - \varphi_d)^2 + \dot{\theta}^2 + (\theta - \theta_d)^2 + \dot{\psi}^2 + (\psi - \psi_d)^2] \tag{30}$$

Equation (31) gives the derivative of V(x).

$$\dot{V}(x) = [(\varphi - \varphi_d)\dot{\varphi} + \ddot{\varphi}\dot{\varphi} + (\theta - \theta_d)\dot{\theta} + \ddot{\theta}\dot{\theta} + (\psi - \psi_d)\dot{\psi} + \ddot{\psi}\dot{\psi}] \tag{31}$$

Functions of angle and position defined in (17-22) could be simplified under perfect cross configuration VTOL (I_x=I_y) condition, while the quadrotor close to point of equilibrium (w_r = 0, $\dot{\psi}=0,\ \dot{\theta}=0,\ \dot{\varphi}=0$) and equation (32) is obtained:

$$\dot{V}(x)=(\varphi-\varphi_d)\dot{\varphi}+\dot{\varphi}\frac{l}{I_x}U_2+(\theta-\theta_d)\dot{\theta}+\dot{\theta}\frac{l}{I_y}U_3 \\ +(\psi-\psi_d)\dot{\psi}+\dot{\psi}\frac{l}{I_z}U_4 \tag{32}$$

The system's controller inputs are defined as below for the stability condition.

$$U_2=-\frac{I_x}{l}(\varphi-\varphi_d)-k_1\dot{\varphi} \tag{33}$$

$$U_3=-\frac{I_y}{l}(\theta-\theta_d)-k_2\dot{\theta} \tag{34}$$

$$U_4=-I_z(\psi-\psi_d)-k_3\dot{\psi} \tag{35}$$

By substituting the above U_2, U_3 and U_4 control inputs in equation (32), the equation can be rewritten as follows:

$$\dot{V}(x)=-\dot{\varphi}^2\frac{l}{I_x}k_1-\dot{\theta}^2\frac{l}{I_y}k_2-\dot{\psi}^2\frac{l}{I_z}k_3 \tag{36}$$

Here, k_1, k_2 and k_3 indicate positive coefficients given from the equations (33) to (36) which are only negative semidefinite. Basic stability for the point of equilibrium is ensured by Lyapunov theorem. Asymptotic stability is provided by using the LaSalle's invariance principle because controlled maximum invariant set of subsystem in $S=\left\{X\in R^6:\dot{V}\mid x=0\right\}$ is restricted by point of equilibrium (Chitour et al., 2020). For the altitude controller, Lyapunov equation and its time derivative are represented in equations (37) and (38).

$$V(x)=\frac{1}{2}[(z-z_d)^2+\dot{z}^2] \tag{37}$$

$$\dot{V}(x)=(z-z_d)\dot{z}+\dot{z}(g-(\cos\theta\cos\varphi)\frac{U_1}{m}) \tag{38}$$

U_1 controller input is defined as in equation (39) for the stability condition.

$$U_1=-\frac{m}{\cos\theta\cos\varphi}(z_d-z-g)-k_z\dot{z} \tag{39}$$

When U_1 control input is substituted in (38), equation (40) is obtained. k_z is the positive coefficient given by (39) that is negative semi-definite.

$$\dot{V}(x)=-\dot{z}^2\frac{k_z}{m}(\cos\theta\cos\varphi) \tag{40}$$

Lyapunov-based controller's parameters are presented in Table 3. k_1, k_2 and k_3 represent coefficients of roll, pitch and yaw angle controllers, respectively. k_z symbolizes the coefficient of altitude controller.

Table 3. Lyapunov-based controller coefficients

Coefficient	Value
k_1	0.167
k_2	0.168
k_3	0.104
k_z	2.15

3.3 Backstepping Controller Design

In this part, the design of the proposed backstepping controller is explained. The altitude and attitude of the quadrotor are controlled by a backstepping controller. This control technique is an adaptive control used in nonlinear dynamical systems (Jin et al., 2022). Backstepping control stands on a recursive design process that links the choice of the Lyapunov equation with feedback control system and enables a strict feedback to achieve asymptotic stability. Lyapunov's direct method is combined with principles of adaptive control in this paper. First, a tracking error is defined in equation (41).

$$z_1=\varphi_d-\varphi \tag{41}$$

The Lyapunov function and its derivative for the above variable are expressed in equations (42) and (43).

$$V(z_1)=\frac{1}{2}{z_1}^2 \tag{42}$$

$$\dot{V}(z_1)=z_1(\dot{\varphi}_d-\dot{\varphi}) \tag{43}$$

Since the time derivative of Lyapunov function must be negative semi-definite, the new virtual controller input $\dot{\varphi}$ is described to stabilize z_1 equation as in equation (44).

$$\dot{\varphi}=\dot{\varphi}_d+a_1z_1 \tag{44}$$

a_1 constant must be positive to get negative semi-definitiveness. Whenever this virtual controller input is substituted in (43), the following equation is obtained:

$$\dot{V}(z_1)=-a_1{z_1}^2 \tag{45}$$

The other change of the employed variable is defined in equation (46):

$$z_2=\dot{\varphi}-\dot{\phi}_d-a_1z_1 \tag{46}$$

After these changes, augmented Lyapunov function could be written as in equation (47):

$$V(z_1, z_2) = \frac{1}{2} z_1^{\,2} + \frac{1}{2} z_2^{\,2} \tag{47}$$

Time derivative of the above Lyapunov function can be written as in equation (48):

$$\dot{V}(z_1, z_2) = -a_1 z_1^{\,2} - z_1 z_2 + z_2 \ddot{\varphi} - z_2 (\ddot{\varphi}_d - a_1 (z_2 + a_1 z_1)) \tag{48}$$

According to the equation (20), $\ddot{\varphi}$ variable can be rewritten as follows:

$$\ddot{\varphi} = \dot{\psi}\dot{\theta} a_1 + a_2 \dot{\theta} w_r + \frac{l}{I_x} U_2 \tag{49}$$

U_2 control input is defined as in (50) under $\ddot{\varphi} = 0$, $\ddot{\varphi} = 0$, $\ddot{\theta}_d = 0$ and $\dot{V}(z_1, z_2) < 0$ conditions.

$$U_2 = \frac{I_x}{l} (z_1 - a_1 \dot{\theta}\dot{\psi} - a_2 \dot{\theta} w_r - a_1 (z_2 + a_1 z_1) - a_2 z_2) \tag{50}$$

The $a_2 z_2$ term with $a_2 > 0$ is added to stabilize z_1. Using the same steps, U_3 and U_4 inputs which control pitch and yaw are defined in equations (51) and (52):

$$U_3 = \frac{I_y}{l} (z_3 - a_3 \dot{\varphi}\dot{\psi} - a_4 \dot{\varphi} w_r - a_3 (z_4 + a_3 z_3) - a_4 z_4) \tag{51}$$

$$U_4 = I_z (z_5 - a_5 \dot{\varphi}\dot{\theta} - a_5 (z_6 + a_5 z_5) - a_6 z_6) \tag{52}$$

The equations from (53) to (56) give variables used in U_3 and U_4 control inputs.

$$z_3 = \theta_d - \theta \tag{53}$$

$$z_4 = \dot{\theta} - \dot{\theta}_d - a_3 z_3 \tag{54}$$

$$z_5 = \psi_d - \psi \tag{55}$$

$$z_6 = \dot{\psi} - \dot{\psi}_d - a_5 z_5 \tag{56}$$

The controller's tracking error for altitude is given as z_7.

$$z_7 = z - z_d \tag{57}$$

The Lyapunov equation for z_7 and its derivative are defined in equations (58) and (59).

$$V(z_7) = \frac{1}{2} z_7^{\,2} \tag{58}$$

$$\dot{V}(z_7) = z_7 (\dot{z}_d - \dot{z}) \tag{59}$$

The x_8 virtual controller input is described as below for stabilizing the z_7 function.

$$x_8 = \dot{z}_d + a_7 z_7 \tag{60}$$

The other variable change is expressed in equation (61):

$$z_8 = x_8 - \dot{z}_d - a_7 z_7 \tag{61}$$

After variable changes are made, the new Lyapunov function is written as below:

$$V(z_7, z_8) = \frac{1}{2} z_7^{\,2} + \frac{1}{2} z_8^{\,2} \tag{62}$$

The derivative of the Lyapunov equation above is expressed in equation (63):

$$\dot{V}(z_7, z_8) = -a_7 z_7^{\,2} - z_7 z_8 + z_8 x_8 - z_8 (\ddot{z}_d - a_7 (z_8 + a_7 z_7)) \tag{63}$$

Time derivative of the x_8 virtual controller input is represented as in equation (64):

$$\dot{x}_8 = g - \cos\theta \cos\varphi \frac{U_1}{m} \tag{64}$$

The U_1 control input which controls the altitude is expressed as the following equation:

$$U_1 = \frac{m}{\cos\theta \cos\varphi} (z_7 + g - a_7 (z_8 + a_7 z_7) - a_8 z_8) \tag{65}$$

Table 4 illustrates the constants of the backstepping control design.

Table 4. Backstepping controller coefficients

Variable	Roll	Pitch	Yaw	Altitude
(a_1,a_2,a_3,a_4, a_5,a_6,a_7,a_8)	(8.6, 6.9)	(8.1, 3.9)	(8.4, 4.1)	(1.4, 5.9)

4. Simulation Results

In this section, trajectory tracking simulations were made under pink noise and sinusoidal distortion. Simulations were performed using MATLAB software. In the context of these simulations, the performance of proposed backstepping controller is compared with the performance of the PID and Lyapunov-based controllers. Robustness analysis was performed by comparing rise time, settling time and overshoot data for all three controller designs. As a result of the comparative analysis, the robustness of the proposed backstepping controller has been proven. Rise time is the time required for a pulse to rise from 10 percent to 90 percent of its steady value. Settling time is the time required for the output to reach a given tolerance band (5% in this paper) and steady within it. Overshoot is the occurrence of a signal

exceeding its target. Overshoot is calculated as a percentage, settling time and rise time are calculated in seconds. The altitude is given in meters, and attitude angle references are given in radians. In simulations, vertical axis shows the position and horizontal axis shows the time. The simulations were carried out for 10 seconds. The altitude and angle references and controllers are illustrated in different colours in the graphs. The blue line is the altitude or angle reference, the red line is PID controller, the yellow line is Lyapunov-based controller, and the purple line is backstepping controller. The model designed in the computer environment consists of various subsystems. In Figure 3, a block representation of the system designed using MATLAB and Simulink is given. The disturbances applied to the controller are also illustrated in Figure 3.

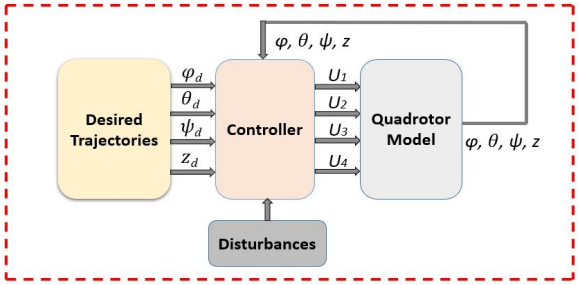

Figure 3. Schematic representation of the proposed system

Desired altitude (z_d) and attitude $(\varphi_d, \theta_d, \psi_d)$ values are produced by the Desired Trajectories. The controller receives the desired values and produces control inputs (U_1, U_2, U_3, U_4) and calculates error by obtaining difference between current trajectories $(z, \varphi, \theta, \psi)$ and desired trajectories $(z_d, \varphi_d, \theta_d, \psi_d)$. The controller tries to decrease error to 0 under disturbances.

4.1 Simulations under Pink Noise

In this subsection, the performance of classical PID is compared to that of the Lyapunov-based and backstepping controller structures for tracking altitude and attitude under pink noise is compared. A pink noise with 0.1 s sample time is implemented into the system. A comparative analysis was carried out after obtaining the time response data for the three controller designs. Figure 4 shows the altitude tracking simulation for the employed controllers under pink noise.

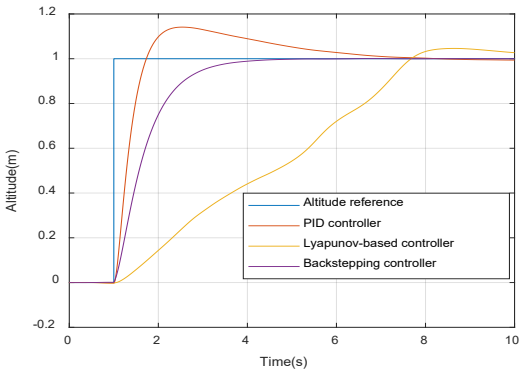

Figure 4. Altitude tracking with pink noise

Figures 5 to 7 show attitude angles tracking simulations under pink noise.

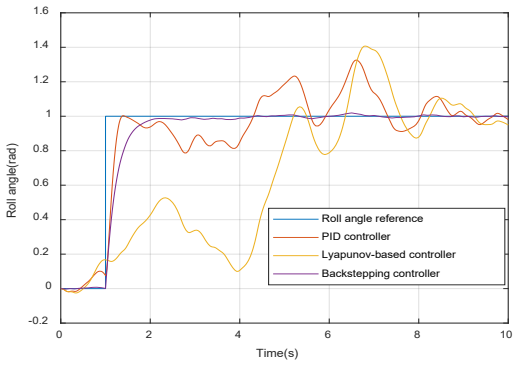

Figure 5. Roll tracking with pink noise

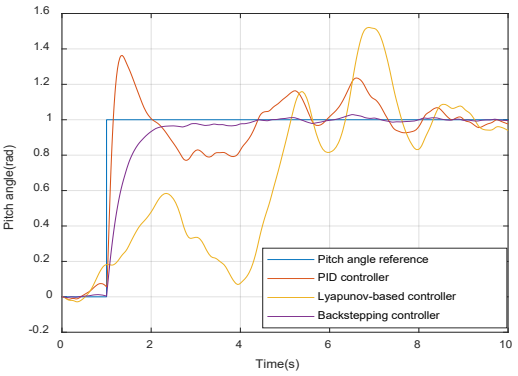

Figure 6. Pitch tracking with pink noise

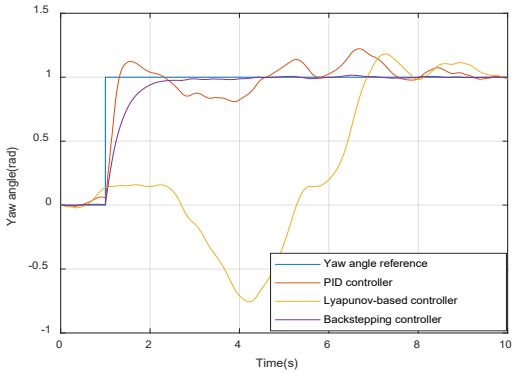

Figure 7. Yaw tracking with pink noise

Table 5. Time response for controllers under pink noise

Controller type	Rise time (s)	Overshoot (%)	Settling time (s)
Roll angle PID contr.	0.26	32.7	8.59
Roll angle Lyapunov-based contr.	4.31	40.8	9.04
Roll angle Backstepping contr.	0.52	1.8	1.78
Pitch angle PID contr.	0.11	36.3	8.53
Pitch angle Lyapunov-based contr.	4.27	52.2	9.67
Pitch angle Backstepping contr.	0.8	2.9	2.12
Yaw angle PID contr.	0.23	22.3	8.6
Yaw angle Lyapunov-based contr.	5.85	18.2	9.3
Yaw angle Backstepping contr.	0.78	1.6	2.04
Altitude PID contr.	0.5	14	5.1
Altitude Lyapunov-based contr.	5.45	4.7	7.41
Altitude Backstepping contr.	1.43	0	3.02

Table 5 shows the time response data for the three controllers. In Table 5, "contr." is the abbreviation for controller. When the altitude and attitude simulations are examined, it can be noted that the backstepping controller is more robust than the other two controllers. Backstepping control design has a very small overshoot and, in the case of altitude tracking, no overshoot. It also has the shortest settling time. Although PID controller has the shortest rise time, it shows a high overshoot and has a longer settling time than the backstepping controller. Lyapunov-based controller has the highest overshoot, highest rise time and highest settling time.

4.2 Simulations under Sinusoidal Disturbance

In this subsection, trajectory tracking performance of the three controllers under sinusoidal disturbance is investigated. A sinusoidal disturbance with an amplitude of 1 and a frequency of 0.001 rad/s is implemented into the system. Time response for controllers was obtained and a comparative robustness analysis was performed. Figure 8 shows the altitude tracking simulation for the employed controllers under the sinusoidal disturbance.

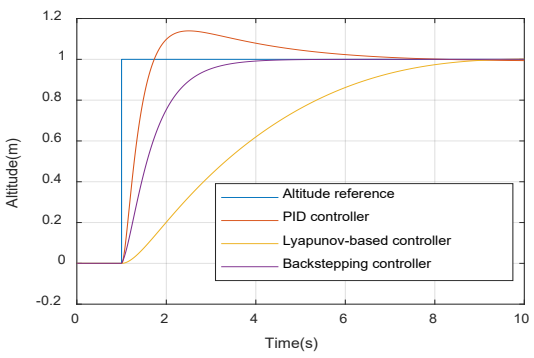

Figure 8. Altitude tracking with sinusoidal distortion

Figures 9 to 11 show the attitude angle tracking simulations under the sinusoidal disturbance.

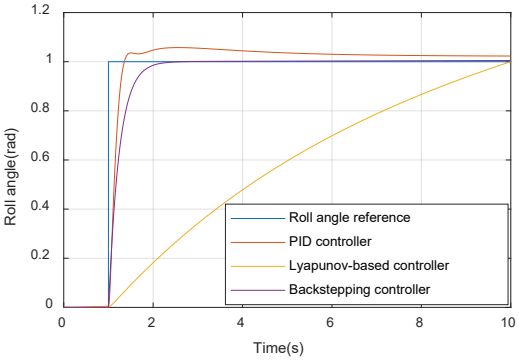

Figure 9. Roll tracking with sinusoidal distortion

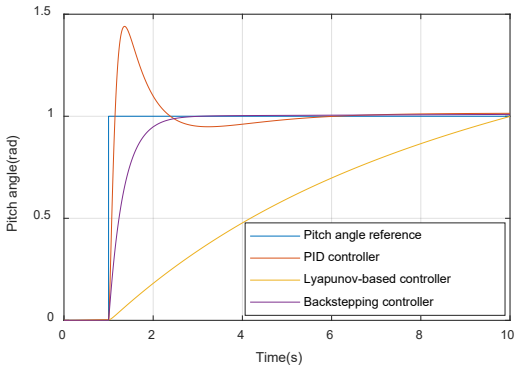

Figure 10. Pitch tracking with sinusoidal distortion

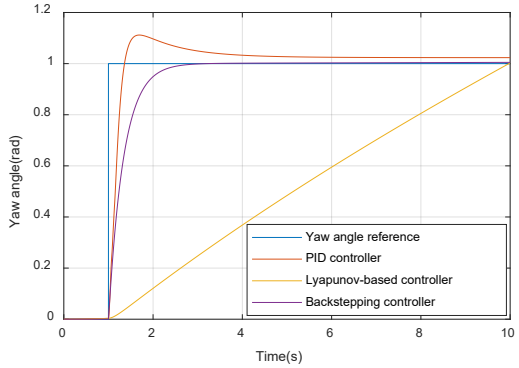

Figure 11. Yaw tracking with sinusoidal distortion

Table 6. Time response of controllers under sinusoidal distortion

Controller type	Rise time (s)	Overshoot (%)	Settling time (s)
Roll angle PID contr.	0.21	6	3.3
Roll angle Lyapunov-based contr.	7.35	0	9.19
Roll angle Backstepping contr.	0.52	0.5	1.7
Pitch angle PID contr.	0.1	44.1	2.17
Pitch angle Lyapunov-based contr.	6.91	0	9.2
Pitch angle Backstepping contr.	0.73	1	2
Yaw angle PID contr.	0.28	11.2	2.92
Yaw angle Lyapunov-based contr.	7.11	0	9.42
Yaw angle Backstepping contr.	0.71	0.5	2
Altitude PID contr.	0.49	13.8	4.77
Altitude Lyapunov-based contr.	4.87	0.2	7.36
Altitude Backstepping contr.	1.07	0	2.95

Table 6 contains data on the time response of the three controllers. When the simulations are analysed, it is revealed that the backstepping controller is the most robust controller. Backstepping control design has a very small overshoot and, in the case of altitude tracking, no overshoot and it has the shortest settling time. Although the PID controller has the shortest rise time, it is also the controller with the highest overshoot. Also, its settling time is longer than that of the backstepping controller. The Lyapunov-based controller has the longest rise time. The Lyapunov-based controller also has the longest settling time, although it has no overshoot.

5. Conclusion

This study firstly explains nonlinear modelling of a quadcopter. This model was created with MATLAB software. Then, three controllers were implemented in order to control height and attitude of the employed UAV. First of all, PID and Lyapunov-based controller designs were presented. Afterwards, this paper set forth the design of the robust backstepping controller, which was developed for controlling the employed quadrotor. To test the robustness of these controllers, pink noise, which is the background noise in electronic devices, and sinusoidal disturbance were given to the system. In order to prove the robustness of the proposed backstepping controller, a comparative robustness analysis was performed which involved the classical PID controller and the Lyapunov-based controller. For this purpose, time response data for all three controllers was obtained. Tables related to the time response of the employed controllers were created using the obtained results. Backstepping controller has the lowest overshoot and shortest settling time. Although the classical PID control structure has a short rise time, it features a high overshoot and has a long settling time. Lyapunov-based controller has the longest rise time and longest settling time and shows a high overshoot under pink noise. As such, the backstepping controller proves to be more robust than the classical PID and Lyapunov-based controllers.

REFERENCES

AL-Qrimli, H. F., D'souza, L. & Hussein, O. D. (2021) An Innovative Approach to a Hybrid Quadrotor Design. *Journal of Robotics and Control (JRC)*. 2(1), 19-23.

Aminifar, F. & Rahmatian, F. (2020) Unmanned aerial vehicles in modern power systems: technologies, use cases, outlooks, and challenges. *IEEE Electrification Magazine*. 8(4), 107-116. doi: 10.1109/MELE.2020.3026505.

Antonelli, G., Cataldi, E., Arrichiello, F., Giordano, P. R., Chiaverini, S. & Franchi, A. (2018) Adaptive trajectory tracking for quadrotor MAVs in presence of parameter uncertainties and external disturbances. *IEEE Transactions on Control Systems Technology*. 26(1), 248-254. doi: 10.1109/TCST.2017.2650679.

Babaie, M., Abarzadeh, M. & Al-Haddad, K. (2022) An Improved High-Resolution Wide Bandwidth ANPC Converter using VLMM and Lyapunov Stability Theory for Grid-Connected Applications. In: *2022 IEEE Energy Conversion Congress and Exposition (ECCE), October 9-13, 2022, Detroit, USA*. pp. 1-6.

Bouadi, H., Aoudjif, A. & Guenifi, M. (2015) Adaptive flight control for quadrotor UAV in the presence of external disturbances. In: *2015 6th International Conference on Modeling, Simulation, and Applied Optimization, ICMSAO 2015, May 27-29, 2015, Istanbul, Turkey*. pp. 1-6.

Boukoberine, M. N., Zhou, Z. & Benbouzid, M. (2019) A critical review on unmanned aerial vehicles power supply and energy management: Solutions, strategies, and prospects. *Applied Energy*. 255, 1-22. doi: 10.1016/j.apenergy.2019.113823

Chitour, Y., Marx, S. & Prieur, C. (2020) Lp-asymptotic stability analysis of a 1D wave equation with a nonlinear damping. *Journal of Differential Equations*. 269(10), 8107-8131.

Darvishpoor, S., Roshanian, J., Raissi, A. & Hassanalian, M. (2020) Configurations, flight mechanisms, and applications of unmanned aerial systems: A review. *Progress in Aerospace Sciences*. 121, 100694. doi: 10.1016/j.paerosci.2020.100694.

Guardeño, R., López, M. J. & Sánchez, V. M. (2019) MIMO PID controller tuning method for quadrotor based on LQR/LQG theory. *Robotics*. 8(2), 36. doi: 10.3390/robotics8020036.

Jiao, Q., Liu, J., Zhang, Y. & Lian, W. (2018) Analysis and design the controller for quadrotors based on PID control method. In: *2018 33rd Youth Academic Annual Conference of Chinese Association of Automation, YAC 2018, May 18-20, 2018, Nanjing, China*. Institute of Electrical and Electronics Engineers (IEEE). pp. 88-92.

Jin, Y., Xiao, Q., Jia, H., Mu, Y., Ji, Y., Teodorescu, R. & Dragičević, T. (2022) A dual-layer back-stepping control method for Lyapunov stability in modular multilevel converter based STATCOM. *IEEE Transactions on Industrial Electronics*. 69(3), 2166-2179. doi: 10.1109/TIE.2021.3063973.

Karahan, M. & Kasnakoglu, C. (2021) Modeling a Quadrotor Unmanned Aerial Vehicle and robustness analysis of different controller designs under parameter uncertainty and noise disturbance. *Journal of Control Engineering and Applied Informatics*. 23(4), 13-24.

Li, G., Wei, P., Yang, W. & Gao, R. (2021) Research on Improved Particle Swarm Optimized Fuzzy PID Control for Quadrotor UAV. In: *2021 China Automation Congress, CAC 2021, October 22-24, 2021, Beijing, China*. Institute of Electrical and Electronics Engineers (IEEE). pp. 7212-7217.

Li, Z., Ma, X. & Li, Y. (2020) Robust trajectory tracking control for a quadrotor subject to disturbances and model uncertainties. *International Journal of Systems Science*. 51(5), 839-851.

Lucas, K. E., Pagano, D. J., Vaca-Benavides, D. A., Garcia-Arcos, R., Rocha, E. M., Medeiros, R. L. & Rios, S. J. (2020) Robust Control of Interconnected Power Electronic Converters to Enhance Performance in DC distribution systems: A case of study. *IEEE Transactions on Power Electronics*. 36(4), 4851-4863. doi: 10.1109/TPEL.2020.3019402.

Ma, J. & Ji, R. (2016) Fuzzy PID for quadrotor space fixed-point position control. In: *2016 Sixth International Conference on Instrumentation & Measurement, Computer, Communication and Control, IMCCC 2016, July 21-23, 2016, Harbin, China.* pp. 721-726.

Mahfouz, M., Taiomour, A., Ashry, M. M. & Elnashar, G. (2021) PID tuning approaches for quadrotors unmanned aerial vehicles. In: *IOP Conference Series: Materials Science and Engineering, 1172 (The 19th International Conference on Aerospace Sciences & Aviation Technology, ASAT-19, April 6-8, 2021, Cairo, Egypt)*. pp. 012040.

Noordin, A., Basri, M. & Mohamed, Z. (2020) Simulation and experimental study on PID control of a quadrotor MAV with perturbation. *Bulletin of Electrical Engineering and Informatics*. 9(5), 1811-1818. doi: 10.11591/eei.v9i5.2158.

Sabour, M. H., Jafary, P. & Nematiyan, S. (2022) Applications and classifications of unmanned aerial vehicles: A literature review with focus on multi-rotors. *The Aeronautical Journal*. 127(1309), 1-25. doi: 10.1017/aer.2022.75.

Shraim, H., Awada, A. & Youness, R. (2018) A survey on quadrotors: Configurations, modeling and identification, control, collision avoidance, fault diagnosis and tolerant control. *IEEE Aerospace and Electronic Systems Magazine*. 33(7), 14-33. doi: 10.1109/MAES.2018.160246.

Tran, H. T., Tran, D. L., Nguyen, V. Q., Do, H. T. & Nguyen, M. T. (2022) A Novel Framework of Modelling, Control, and Simulation for Autonomous Quadrotor UAVs Utilizing Arduino Mega. *Wireless Communications and Mobile Computing*. 2022, 1-17. doi: 10.1155/2022/3044520.

Vanitha, N. S., Manivannan, L., Meenakshi, T. & Radhika, K. (2020) Stability analysis of quadrotor using state space mathematical modeling. *Materials Today: Proceedings*. 33(7), 4040-4043. doi: 10.1016/j.matpr.2020.06.428.

Xian, B., Zhao, B., Zhang, Y. & Zhang, X. (2017) A low-cost hardware-in-the-loop-simulation testbed of quadrotor UAV and implementation of nonlinear control schemes. *Robotica*. 35(3), 588-612. doi: 10.1017/S0263574715000727.

Yaacoub, J. P., Noura, H., Salman, O. & Chehab, A. (2020) Security analysis of drones systems: Attacks, limitations, and recommendations. *Internet of Things*. 11, 100218. doi: 10.1016/j.iot.2020.100218.

Zabidin, Y. A. A., Pairan, M. F. & Shamsudin, S. S. (2020) Dynamic Modelling and Control for Quadcopter UAV with LabVIEW and X-Plane Flight Simulator. *Journal of Complex Flow*. 2(2), 19-26.